IEEE Access
Multidisciplinary | Rapid Review | Open Access Journal

Received September 1, 2019, accepted October 14, 2019, date of publication October 24, 2019, date of current version November 6, 2019.

Digital Object Identifier 10.1109/ACCESS.2019.2949336

A Competitive-Cooperative Game Method for Multi-Objective Optimization Design of a Horizontal Axis Wind Turbine Blade

RUI MENG[1,2] AND NENG-GANG XIE[3]

[1]College of Mechanics and Materials, Hohai University, Nanjing 210098, China
[2]School of Mechanical Engineering, Anhui University of Technology, Ma'anshan 243002, China
[3]School of Management Science and Engineering, Anhui University of Technology, Ma'anshan 243002, China

Corresponding author: Neng-Gang Xie (xienenggang@aliyun.com)

This work was supported by the National Natural Science Foundation of China under Grant 51605005.

ABSTRACT This paper presents a multi-objective optimization model of a wind turbine blade based on blade's parameterized finite element model, where annual energy production and blade mass are the objective functions, and aerodynamic and structural parameters are the design variables. In this study, the maximum axial thrust, strain, displacement, and first-order natural frequency of blade are selected as constraints. A novel competitive-cooperative game method is proposed to obtain the optimal preference solution. In this method, a new exploration method of player's strategy space named 'correlation analysis under fuzzy k-means clustering' is proposed, and the payoff functions are constructed according to competitive and cooperative behaviors. Two optimization schemes with preference objectives are obtained and all goals showed clear improvements over the initial solutions, and this method reveals the relationship between blade shape and desired performance. More deeply, dynamic sensitivities of various design variables to objective functions are obtained for different blade shapes.

INDEX TERMS Competitive-cooperative game, parameterized finite element model of wind turbine blade, aerodynamic and structural design, dynamic sensitivity.

I. INTRODUCTION

In multi-objective optimization issues, each objective restricts and influences each other. There exist two typical methods for obtaining the final optimization solution in multi-objective optimization design of a wind turbine blade. One method is to obtain a large number of non-inferior solutions by using the related method, such as nondominated sorting genetic algorithm II [1], gradient-based multi-objective evolution algorithm [2], or particle swarm optimization [3] and then a final solution can be chosen by the designer. These methods are widely applied and non-inferior solutions provide designers with a comprehensive understanding for the design problem. However, these methods may be time-consuming when a widely distributed non-inferior solution set is required, especially for multi-objective optimization problems with complex constraints. The other main approach uses conventional multi-objective methods, such as hierarchical optimization methods or weighted objectives method to convert multi-objective problems into single-objective problems [4], [5]. These methods can simplify the path to a solution, whereas, an inappropriate evaluation function will get a non-global optimal solution.

Game theory can be used to analyze and attain optimal solutions between individuals with conflicting relationships. From a methodology perspective, the approach effectively reconciles conflicts and contradictions and is similar to multi-objective optimization problems in the field of engineering [6], [7]. The basic idea involves building a game-theoretic model in which all game players eventually generate an equilibrium solution through mutual negotiation and compromise. Game theory belongs to the category of bionic and heuristic algorithms that are derived from simulations of biological phenomena. By analyzing [6]–[8], the following relationships between game models and biological systems can be established: (1) One game player corresponds to one objective function; (2) Profits of game players correspond to the living space of biological populations; (3) Multiple strategy subspaces of game players correspond to different genes of biological populations; (4) Behaviors of game players

The associate editor coordinating the review of this manuscript and approving it for publication was Lei Wu.

correspond to behaviors of biological populations; (5) Game modes correspond to the relational models of biological populations; (6) The game process is based on the survival of the fittest or natural selection process; (7) The final convergent solution of the game corresponds to the stable biological population pattern. Based on the above seven relationships between game theory and biological systems, the technical route of a multi-objective game method can be established as follows [8]: (a) m design objectives are defined as m players and set of design variables $X = \{x_1, x_2, \cdots, x_n\}$ are divided into m strategy spaces, $\{s_1, s_2, \cdots, s_m\}$, owned by each player; (b) A specific game pattern is then constructed by assigning different behaviors to each player, and game pattern is an important factor, to some degree, in determining precision of the game solution and profits of each game player; (c) In each game round, each player seeks its own best strategy in its multiple feasible strategies to make the best payoff functions, where payoff functions are a mapping of objective functions; (d) The final game equilibrium solution can be obtained after several game iterations.

Multi-objective optimization methods based on game theory are suitable for solving many complex engineering problems. Important characteristics of this approach include: (1) The ability to transform complex high-dimensional optimization problems into several relatively simple low-dimensional optimization problems, thereby reducing the difficulty of solving the problem; (2) Compared to traditional multi-objective optimization methods, those based on game theory reveal the sensitivity of sub-objectives to design variables by dividing them into strategy subspaces owned by each player, which is helpful for engineers to optimize the design. A number of researchers have applied a game-theoretic approach to solving multi-objective design problems. For instance, Désidéri [9] implemented an aircraft wing shape optimization using Nash, Stackelberg, and cooperation games. Also, a stochastic Markov game was built to seek for correlated equilibrium between multi-objective workflow [10]. Feng *et al.* [11] proposed a Bayesian game-theoretic method for optimizing the allocation of limited defensive resources. A game-based localized multi-objective topology control scheme was presented to achieves a trade-off among energy consumption, link delay and link lifetime [12]. In addition, Jiang and Liu built a multi-objective Stackelberg game model for water supply networks with incomplete data [13]. Multi-objective optimization based on cooperative game theory was also used by Jing *et al.* [14] to design a neighborhood-level urban energy network. Nwulu and Xia [15] applied game theory to multi-objective optimization for dynamic economic emission dispatch. Besides, a dynamic game theory-based two-layer scheduling method was developed to achieve multi-objective flexible job scheduling [16]. Xiao *et al.* [17] demonstrated a new approach based on gene expression programming and Nash equilibrium for the multi-objective optimization of thin-walled pressure vessels and the hull form parameter design of a small-water-plane-area twin hull. Xie *et al.* [18] proposed a method based on evolutionary game theory for vehicle suspension design. Through the related analysis, it can be seen that (a) player's behavior mode mainly includes competition type and cooperation type; and (b) the game optimization solution has well calculation accuracy; (c) the cooperative behavior of some players is beneficial to the acquisition of collective interests.

Herein, a novel competitive-cooperative game theoretic method is proposed. As a proof of principle, an aerodynamic and structural model of a horizontal axis wind turbine (HAWT) blade is optimized. The rest of this paper is organized as follows: In Section II, competitive-cooperative game method is presented; Section III establishes a parameterized finite element model of the HAWT blade; In Section IV, a multi-objective optimization model of the HAWT blade is introduced; Section V presents the results of a real-world HAWT blade along with a detailed discussion; Finally, conclusions are presented in Section VI.

II. COMPETITIVE-COOPERATIVE GAME METHOD

The proposed method comprises two key techniques, i.e., establishment of strategy space exploration method and construction of game pattern. They are explained as follows.

(1) Design variables $X = \{x_1, x_2, \cdots, x_n\}$ are divided into strategy spaces $S = \{S_1, S_2, \cdots, S_m\}$ owned by m players based on the exploration method of the strategy space, where $S_1 = \{x_i, \cdots, x_j\}, \cdots, S_m = \{x_k, \cdots, x_l\}$ and $S_1 \cup \cdots \cup S_m = X; S_a \cap S_b = 0\ (a, b = 1, \cdots m; a \neq b)$. In this study, compared to the static strategy space [18], its advantage lies in that strategy spaces can be adaptively adjusted based on results of the previous iteration.

(2) A competitive-cooperative game pattern is constructed by assigning competitive behavior to one player, whereas cooperative behavior is assigned to other players, which can reflect the preference of the designer. Namely, if the designer prefers one objective function, competitive behavior is assigned to this objective function, whereas cooperative behavior is assigned to all the other objective functions.

A. ESTABLISHMENT OF STRATEGY SPACE EXPLORATION METHOD

Arguably, the first critical step in multi-objective game theoretic methods is decomposing design variables into strategy spaces owned by each player. One important contribution of this study is that a novel strategy space exploration method, called 'correlation analysis under fuzzy k-means clustering', is proposed based on fuzzy theory and data mining. This method takes the fuzzy membership degree of design variables to the objective functions into account, so decomposition results of strategy spaces is better than k clustering method [19]. Its calculation steps are as follows:

(1) For a given set of design variables $X = \{x_1, x_2, \cdots, x_n\}$ and for any design variable x_j, the effect of x_j on f_i objective can be calculated as (1), as shown at the bottom of the next page, where Δx_j is the step size of x_j.

Normalization produces an impact index $\Delta(j,i)$, defined as

$$\Delta(j,i)=\frac{\zeta(j,i)}{\sum_{l=1}^{n}\zeta(l,i)}\quad(j=1,2,\cdots,n;\ i=1,2,\cdots,m)\quad(2)$$

A higher impact index indicates the design variable is more sensitive to this objective function.

(2) Let the classified sample point set be $\Delta=\{\Delta_1,\Delta_2,\Delta_j,\cdots,\Delta_n\}$. Here, $\Delta_j=\{\Delta(j,1),\Delta(j,2),\cdots,\Delta(j,m)\}$ and Δ_j is the j_{th} impact index set of this design variable on m objective functions.

(3) Since the set of design variables is divided into m subsets owned by each player, the number of clusters is equal to m. Coordinates of the m cluster centers, marked as $\Delta_z^k=\{\Delta_{z1}^k,\cdots,\Delta_{zm}^k\}(k=1,\cdots,m)$, are far away from each other in order to ensure the satisfaction of clustering, where $\Delta_{zi}^k\in[0,1](i=1,2,\cdots,m;\ k=1,2,\cdots,m)$.

(4) The Euclidean distance between the k_{th} cluster center and the j_{th} classified sample point is defined as $d(k,j)$. The degree of membership between the j_{th} sample point and the k_{th} cluster center $s(k,j)$ can be obtained as

$$s(k,j)=\frac{1}{\sum_{i=1}^{m}\left(\frac{d(k,j)}{d(i,j)}\right)^{\frac{2}{q-1}}}\quad(k=1,\cdots,m;j=1,\cdots,n)\quad(3)$$

where q is the fuzzy weighting coefficient.

(5) The new clustering center is calculated by

$$\Delta_z^k=\frac{\sum_{j=1}^{n}s(k,j)^q\Delta_j}{\sum_{j=1}^{n}s(k,j)^q}\quad(k=1,\cdots,m;j=1,\cdots,n)\quad(4)$$

(6) The value function J is calculated as

$$J=\sum_{k=1}^{m}\sum_{j=1}^{n}s(k,j)^q d(k,j)^2\ (k=1,\cdots,m;j=1,\cdots,n)\quad(5)$$

If the change from the previous value function is less than a certain threshold δ, the algorithm returns to Step (7). Otherwise, go back to Step (4).

(7) Coordinates of the m cluster centers are organized into an $m\times m$ matrix, i.e.,

$$\Psi=\begin{bmatrix}\Delta_{z1}^1 & \Delta_{z2}^1 & \cdots & \Delta_{zm}^1\\ \Delta_{z1}^2 & \Delta_{z2}^2 & \cdots & \Delta_{zm}^2\\ \cdots & \cdots & \cdots & \cdots\\ \Delta_{z1}^m & \Delta_{z2}^m & \cdots & \Delta_{zm}^m\end{bmatrix}$$

Design variable subsets in each cluster can be obtained based on the principle of maximum degree of membership. Here, let the subset of design variables in the k_{th} cluster be γ_k.

(8) Find the largest value of Ψ matrix, marked as Δ_{zi}^k, which effectively means the k_{th} cluster has the strongest correlation with the i_{th} design objective. Therefore, the design variable subset in γ_k forms the strategy space S_i owned by the i_{th} design objective.

(9) Delete the k_{th} row and i_{th} column of Ψ matrix where the largest element Δ_{zi}^k is located, and form a new $(m-1)\times(m-1)$ matrix to replace Ψ. Subsequently, loop back to Step (8). The loop termination condition is reached when all strategy spaces are confirmed.

In addition, a supplementary explanation to this method is made as follows: if a design variable only affects one objective function, marked as f_i, and has no effect on all other functions, it can be decomposed directly into strategy space of f_i in advance. Then, the remaining design variables can be decomposed into the strategy space using the proposed method, which can improve the efficiency of dividing the strategy space.

B. CONSTRUCTION OF COMPETITIVE-COOPERATIVE GAME PATTERN

Due to the reason that competitive and cooperative behavior is the most basic behavior mode in biological systems, they are applied to construct the payoff functions. Competitive behavior is motivated by self-interest and its payoff function is

$$u_i=\frac{f_i}{\bar{f}_i}\quad(i=1,2,\cdots,m)\quad(6)$$

where $\bar{f}_i$ is the initial value of objective function i. In Eq. (6), payoff function of competitive behavior only depends on the object function value of self-interest, and does not take the values of other object functions into account. In contrast, cooperative behavior is collectivistic and its payoff function is

$$u_i=\frac{f_i}{5\bar{f}_i}+\sum_{j=1(j\neq i)}^{m}\frac{4f_j}{5(m-1)\bar{f}_j}\quad(i=1,2,\cdots,m)\quad(7)$$

In Eq. (7), payoff function of cooperative behavior not only depends on the object function value of self-interest, but also takes the values of other object functions into account. Herein, the ratio of selfish factor to altruistic factor is 0.25. In this study, a competitive-cooperative game pattern is constructed, where one player is endowed competitive behavior and its payoff function is constructed based on Eq. (6) and other objectives are endowed with cooperative behavior, and their payoff functions are constructed based on Eq. (7). This competitive-cooperative game pattern can not only guarantee collective benefit to all players, but also gives priority to one player who exhibits competitive behavior.

$$\zeta(j,i)=\frac{\sum_{l=1}^{2}\left|f_i(x_1,\cdots,x_{j-1},x_j+(l-1)\Delta x_j,x_{j+1},\cdots x_n)-f_i(x_1,\cdots,x_{j-1},x_j+(l-2)\Delta x_j,x_{j+1},\cdots x_n)\right|}{2\Delta x_j}\quad(1)$$

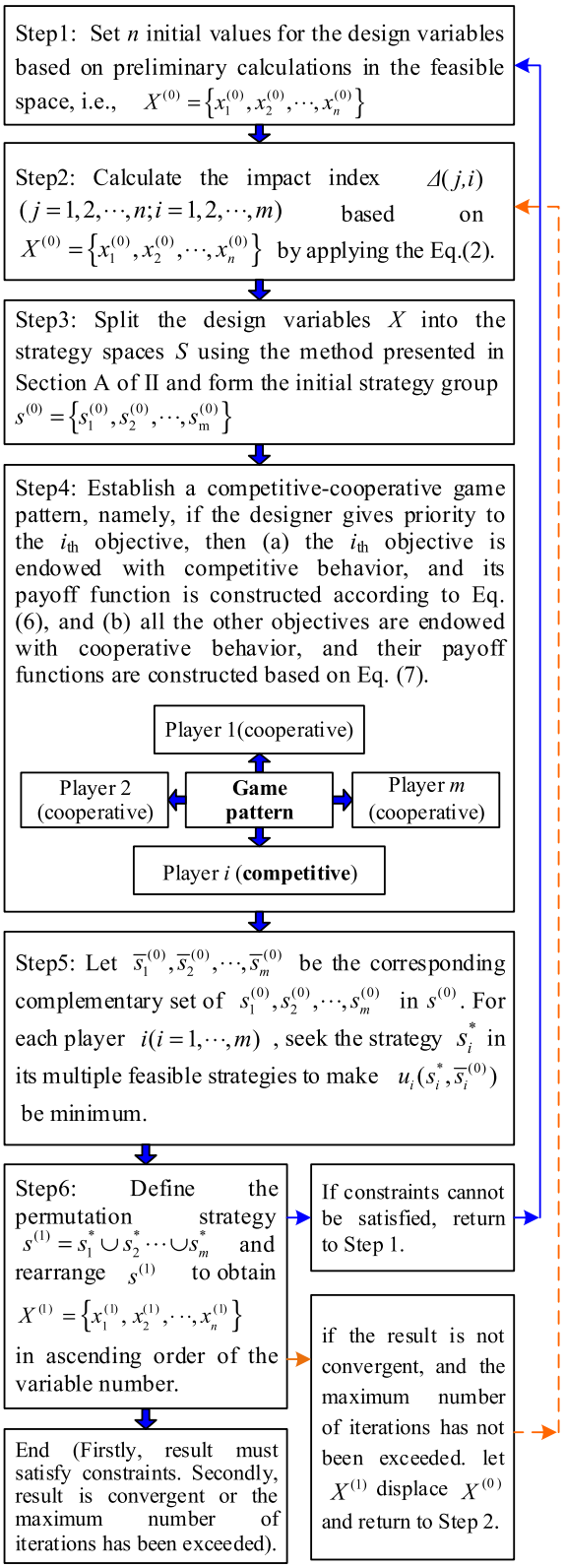

FIGURE 1. Flowchart of the competitive-cooperative game method.

C. SOLUTION STEPS OF COMPETITIVE-COOPERATIVE GAME METHOD

Flowchart of the competitive-cooperative game method is shown in Fig.1.

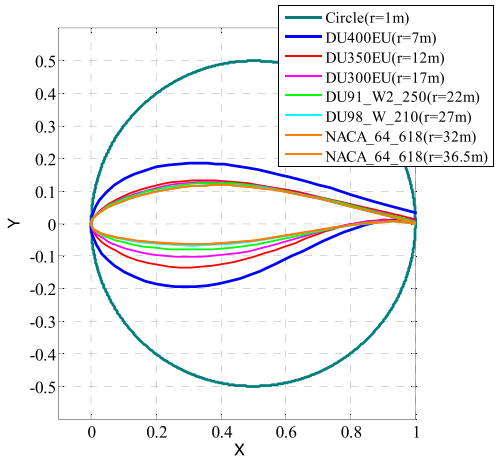

FIGURE 2. Eight single-unit reference airfoils.

III. ESTABLISHMENT OF PARAMETERIZED FINITE ELEMENT MODEL OF A HAWT BLADE

The establishment of a parametric finite element model of the HAWT blade is a prerequisite for the multi-objective aerodynamic and structural optimization of the blade, and it includes five steps as follows.

(1) Set unit reference airfoils and their locations. Analyzing a 1.5-MW wind turbine blade [20], eight single-unit reference airfoils were selected, as shown in Fig.2, where r is the radius at the airfoil section.

(2) Construct all other unit airfoils based on the above eight single-unit reference airfoils shown in Fig. 2. From r = 0–1 m, it was unit circular section. Other unit airfoils were located every 0.5 m along the blade and were derived by spline interpolation based on two adjacent unit reference airfoils, as shown in Eq. (8).

$$(x_D, y_D) = (x_i, \frac{D_i - D}{D_i - D_{i+1}} y_{i+1} + \frac{D - D_{i+1}}{D_i - D_{i+1}} y_i), \quad (i = 1, 2, \cdots, 7) \tag{8}$$

where D is the relative thickness of the airfoil; D_i is the relative thickness of the unit reference airfoils; (x_D, y_D) refers to the coordinate value of an airfoil with relative thickness D; and (x_i, y_i) is the coordinate value of a unit reference airfoil.

(3) Obtain the actual aerodynamic airfoils by making three transformations to unit airfoils, including scaling, translation, and rotation, as shown in Fig. 3. Specific values of three transformations were determined by the actual chord length, aerodynamic center, and twist angle of the airfoil. Herein, the aerodynamic center was fixed in advance, as shown in Fig. 4. Chord length and twist angle of the seven reference airfoil sections from r = 7– 36.5 m were taken as the parameterized design variables. Chord lengths are marked as $x_i(i = 1, \cdots, 7)$ and twist angles are marked as $x_i(i = 8, \cdots, 14)$. The chord length and twist angle of other airfoils were calculated by cubic spline interpolation based on $x_i(i = 1, \cdots, 7)$ and x_i $(i = 8, \cdots, 14)$. Finally,

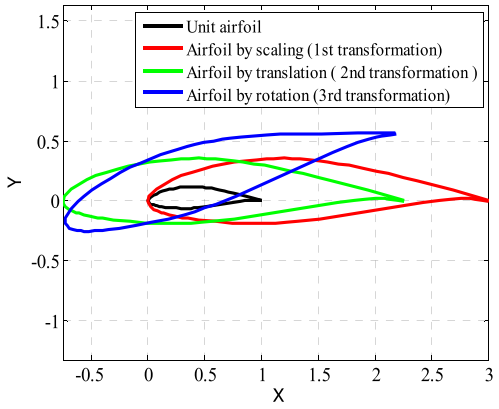

FIGURE 3. Three transformations of the unit airfoil.

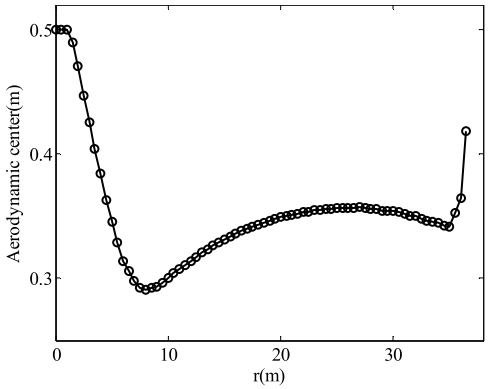

FIGURE 4. Aerodynamic center distribution of blade.

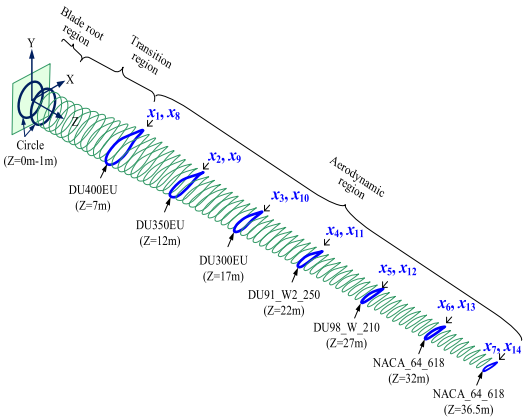

FIGURE 5. Three-dimensional aerodynamic airfoils, including x_i ($i = 1, \cdots, 14$).

the actual three-dimensional aerodynamic airfoils, including $x_i (i = 1, \cdots, 14)$, are shown in Fig. 5, where Z has the same meaning as r.

(4) Set structural cross-section and laminate design. Hollow thin-walled composite structures [20] were used in this study and its cross-section is presented in Fig. 6 [22]. The spar cap is made up of 0° unidirectional glass fiber reinforced plastic (GFRP). The core material contains Polyvinyl chloride (PVC) and balsa wood. The trailing and leading edge

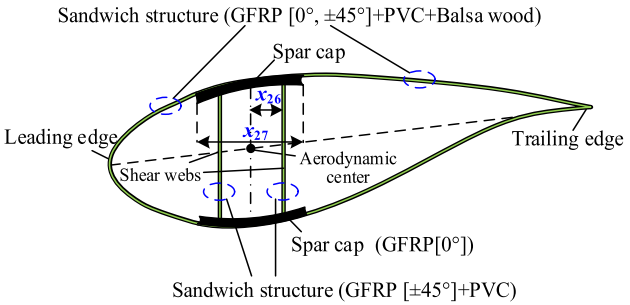

FIGURE 6. Structural cross-section of a blade, including x_i ($i = 26, 27$).

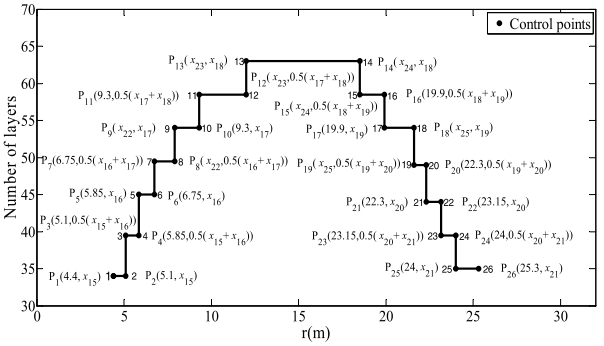

FIGURE 7. Laying setting of the spar cap, including x_i ($i = 15, \cdots, 25$).

are made up of three-directional GFRP (0°, ±45°) as well as core material. Shear webs are made up of bidirectional GFRP (±45°) and PVC. Because the structural performance of the blade is considerably affected by the central areas of the spar cap. Therefore, areas of the spar cap from r = 4.4–25.3 m were selected for optimization. Herein, 26 control points, marked as P_j ($j = 1, \cdots, 26$), were used to effectively simplify the laminate design in this region. Specific layering settings are presented in Fig. 7, where $x_i (i = 15, \cdots, 21)$ is a positive integer referring to the number of layers and $x_i (i = 22, \cdots, 25)$ is the location of the layer. Taking control point 1 as an example, the specific settings were as follows: the location of layers was r = 4.4 m and the number of layers was equal to x_{15}. In addition, the location of the shear web and width of the spar cap can affect the structural performance of the blade significantly, thus the location of the shear web was marked as x_{26} (Fig. 6) and the width of the spar cap was marked as x_{27}(Fig. 6).

(5) Construct the parameterized finite element model of a HAWT blade. To create the finite element model of the blade, SHELL91 and SHELL99 elements were adopted in ANSYS (ANSYS Inc) [20], [22]. The SHELL91 and SHELL99 element was used to simulate the sandwich structures and non-sandwich structures, respectively. The parameterized finite element model can be implemented in ANSYS Parameterized Design Language (APDL) based on the parameters $x_i (i = 1, 2, \cdots, 27)$ defined in the previous four steps. In addition, the blade was treated as a cantilever beam. The parameterized finite element model of the HAWT blade is shown in Fig. 8.

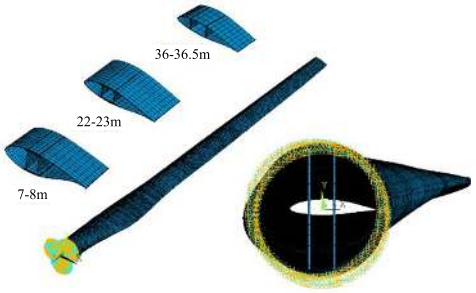

FIGURE 8. Parameterized finite element model of a HAWT blade.

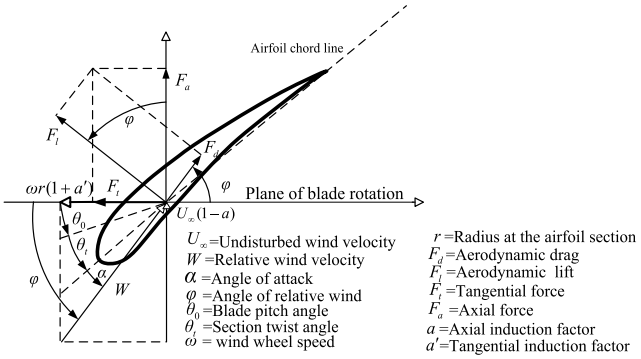

FIGURE 9. Forces acting on a section of the wind turbine blade.

IV. MULTI-OBJECTIVE OPTIMIZATION DESIGN MODEL OF A HAWT BLADE

A. DESIGN VARIABLES AND OBJECTIVE FUNCTIONS

The design variables were obtained in Section III as $x_i(i = 1, 2, \cdots, 27)$. There exist several different design intents and objective function, such as annual energy production (AEP) [21]–[24], rotor thrust or torque [25], power output and vibration of drive train and tower [26], blade mass [3], [27], [28], cost of energy [29]–[31], and cost of composite materials [32]. Herein, according to Step (5) in Section C of II, smaller value of payoff function represents a better design scheme, therefore minus AEP instead of AEP was used as the aerodynamic objective function, and blade mass was applied as the structural objective functions [22].

(1) Aerodynamic objective function

The negative number of AEP is defined as follows.

$$\begin{aligned} f_1(X) &= -\text{AEP} \\ &= -\sum_{i=1}^{N-1} \frac{1}{2}[P(v_{i+1}) + P(v_i)] \\ &\quad \times \Phi(v_i < U_\infty < v_{i+1}) \times 8760 \\ &\rightarrow \min \end{aligned} \tag{9}$$

where N is the number of discrete wind speeds. According to the Weibull wind distribution, the probability of a wind speed ranging from v_i to v_{i+1} can be calculated by $\Phi(v_i < U_\infty < v_{i+1}) = \exp[-(\frac{v_i}{A})^k]$-$\exp[-(\frac{v_{i+1}}{A})^k]$ where k and A are the shape and scale parameter of the wind, respectively, and P is the output power. Forces acting on a section of the wind turbine blade [33] are shown in Fig. 9. The improved blade element momentum (BEM) [34] can be used to solve P, $P = \omega \times \int_0^R dM$ where R is radius of the wind wheel and dM refers to tangential torque of airfoil section. The steps for calculating dM are as follows:

1) Initialize a and a'. Here, set $a = a' = 0$.

2) Compute $\varphi = \arctan \frac{(1-a)U_\infty}{(1+a')\omega r}$.

3) Compute $\alpha = \varphi - (\theta_0 + \theta_t)$.

4) Compute $C_n = C_l \cos\varphi + C_d \sin\varphi$;$C_t = C_l \sin\varphi - C_d \cos\varphi$, where C_l is the lift coefficient and C_d is the drag coefficient.

5) Recalculate $a' = \frac{1}{\frac{8\pi r \chi \sin\varphi \cos\varphi}{cBC_t} - 1}$, where χ is the Prandtl correction factor [34] and B is the number of blades.

6) Recalculate a, based on Eq. (10) [34]:

$$a = \begin{cases} \dfrac{1}{\frac{8\pi r \chi \sin^2\varphi}{cBC_n} + 1}, & a \le a_c \\ \dfrac{1}{2}[2 + K(1 - 2a_c) \\ -\sqrt{[K(1-2a_c)+2]^2 + 4(Ka_c^2 - 1)}], & a > a_c \end{cases} \tag{10}$$

where a_c is threshold value of axial induction factor, and $K = \frac{8\pi r \chi \sin^2\varphi}{cBC_n}$.

7) If the changes in a and a' are greater than a certain allowable deviation, return to Step 2); Otherwise, go to Step 8).

8) Compute $W = \sqrt{U_\infty^2(1-a)^2 + \omega^2 r^2(1+a')^2}$.

9) Compute $dM = \frac{1}{2}B\rho_a W^2 c(C_l \sin\varphi - C_d \cos\varphi)rdr$ where ρ_a is air density.

(2) Structural objective function

A lower blade mass is beneficial for improving the blade structure while complying with the design constraints. Herein, blade mass was employed as the structural objective function.

$$f_2(X) = \sum_k \rho_k \times V_k \rightarrow \min \tag{11}$$

where ρ_k and V_k refers to the density and volume of the k_{th} material.

B. DESIGN CONSTRAINTS

Necessary constraints need to be imposed on the blade design to ensure the blade function. Constraints can be geometric, aerodynamic, or physical. Geometric constraints mainly include ground clearance constraints [35] and displacement and tip deflection constraints [36], [37]; Aerodynamic constraints mostly refer to shell and airfoil thickness demands [38]; Physical constraints mainly include linear inequality bound constraint [3], [29], [31], stress or strain constraints [3], [24], [27], fatigue failure constraint [32], thrust constrain of blade root [39] and natural frequency constraint [3], [27], [30].

In this study, the maximum axial thrust of blade root ($F_{\max}$) was defined as the thrust constraint. The maximum strain ($\varepsilon_{\max}$), maximum displacement of Y direction ($d_{\max}$), and first-order natural frequency (f_{st}) of the blade were defined

TABLE 1. Performance parameters of the composite material.

Material	E_1 (GPa)	E_2 (GPa)	ν_{12}	G_{12} (GPa)	ρ (kg·m^{-3})
Unidirectional GFRP	42.192	12.525	0.240	3.517	1910
Balsa	3.500	0.800	0.300	0.157	151
PVC	0.045	0.045	0.085	0.022	60
Bidirectional GFRP	11.471	11.471	0.614	11.758	1910
Three-directional GFRP-1	31.800	11.400	0.490	6.500	1910
Three-directional GFRP-2	26.900	13.408	0.470	7.532	1910

TABLE 2. Upper and lower limits of design variables.

	$x_{1/m}$	$x_{2/m}$	$x_{3/m}$	$x_{4/m}$	$x_{5/m}$	$x_{6/m}$	$x_{7/m}$	$x_{8/rad}$	$x_{9/rad}$	$x_{10/rad}$	$x_{11/rad}$	$x_{12/rad}$	$x_{13/rad}$	$x_{14/rad}$
Lower limit	2.7	2.5	2.15	1.9	1.7	1.4	1.1	0.12	0.08	0.03	0.01	-0.015	-0.026	-0.037
Upper limit	3.3	2.69	2.49	2.14	1.89	1.69	1.39	0.21	0.119	0.079	0.029	0.009	-0.016	-0.027
	x_{15}	x_{16}	x_{17}	x_{18}	x_{19}	x_{20}	x_{21}	$x_{22/m}$	$x_{23/m}$	$x_{24/m}$	$x_{25/m}$	$x_{26/m}$	$x_{27/m}$	
Lower limit	28	39	49	59	48	41	30	7.0	10.0	16.0	20.5	0.13	0.5	
Upper limit	38	48	58	65	55	47	40	9.0	13.0	19.0	22.0	0.25	0.8	

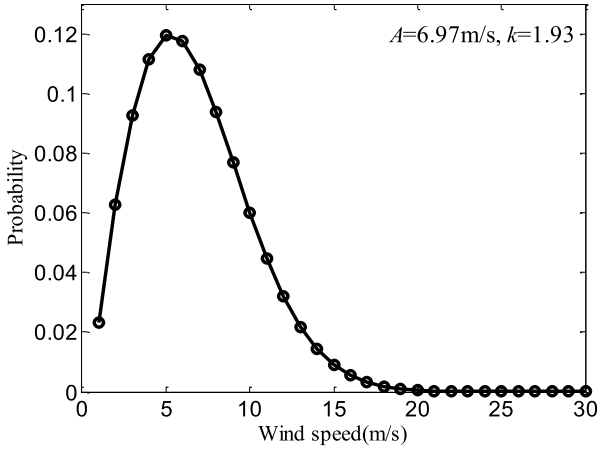

FIGURE 10. Wind speed probability distribution.

as the strength, stiffness, and stability constraints [22], respectively.

$$\begin{cases} F_{\max} \leq [F] \\ \varepsilon_{\max} \leq [\varepsilon] \\ d_{\max} \leq [d] \\ |f_{st} - 3f_{rot}| \geq \nabla \end{cases} \tag{12}$$

where $[F]$ refers to the allowable axial thrust of blade root, $[\varepsilon]$ is the allowable strain, $[d]$ is the allowable displacement of Y direction, f_{rot} is the rotation frequency of the wind wheel, and ∇ is the tolerance of the first-order natural frequency. In addition, all design variables must satisfy upper and lower limits.

V. EXAMPLE BASED ON A REAL-WORLD HAWT BLADE

A. CALCULATION STATEMENT

Basic parameters of wind turbine design were: (1) Three blades; (2) A rated wind speed of 12 m/s, cut-in of 4 m/s and cut-out wind speeds of 25 m/s, respectively; (3) Air density of 1.225 kg·m^{-3}. Herein, a Weibull wind distribution was adopted for the wind speed distribution model, as shown in Fig. 10. Performance parameters of the composite material are shown in Table 1 [22], where E refers to the modulus of elasticity, ν is Poisson's ratio, and G is the shear modulus.

The design variables, objective functions, and constraints were defined in Section IV. According to the design requirements, $[F] = 200$kN, $[\varepsilon] = 0.005$, $[d] = 5.5$ m, $f_{rot} = 0.317$ Hz, and $\nabla = 0.03$ Hz and the upper and lower limits of the design variables are listed in Table 2 [22].

B. COMPUTATION RESULTS AND ANALYSIS

If a designer would like to not only improve the collective profit of aerodynamic and structural performance, but also give priority to aerodynamic performance, u_1 is constructed according to Eq. (6) and u_2 is constructed according to Eq. (7). The final optimal solution with AEP preference (X_{AEP}) was obtained after 12 rounds based on the steps presented in Section C of II. The iterative process, which began with an initial design ($X_{Initial}$), is shown in Table 3. Herein, $\eta = (x_{15}, x_{16}, \cdots, x_{27})$. Because η only affects f_2, it can be assigned to S_2 in advance according to the supplementary explanation of the strategy space exploration method presented in Section A of II.

Similarly, if the designer would like to improve collective profit of aerodynamic and structural performance, and prioritize structural performance, u_2 is constructed according to Eq. (6) and u_1 is constructed according to Eq. (7). The final optimal solution with blade mass preference (X_{Mass}) was obtained after 10 rounds based on the solution steps presented in Section C of II. Results of the iterative process are presented in Table 4. In addition, a comparison of the main performance parameters is listed in Table 5. The $X_{Initial}$, X_{AEP} and X_{Mass} are as follows:

$X_{Initial}$ = [3.2864, 2.6101, 2.2135, 1.9459, 1.7733, 1.5376, 1.2374, 0.1287, 0.0837, 0.0486, 0.0171, -0.0059, -0.0253,

-0.0362, 37, 46, 57, 65, 52, 44, 39, 7.2534, 12.7718, 18.9249, 20.8367, 0.1333, 0.7135];

TABLE 3. Iterative process for X_{AEP}.

Game rounds	Behavior of game player		Strategy space		Objective function values	
	u_1	u_2	S_1	S_2	f_1 (kWh)	f_2 (kg)
Initial design	——	——	——	——	-3777346	7210
1	competition	cooperation	$x_{14},x_{13},x_{12},x_{11},x_{10},x_6$	$x_1,x_9,x_2,x_3,x_4,x_5,x_8,x_7,\eta$	-3812922	7072
2	competition	cooperation	$x_{14},x_{13},x_{12},x_{11},x_6,x_7,x_{10}$	$x_1,x_3,x_2,x_4,x_5,x_8,x_9,\eta$	-3871296	6858
3	competition	cooperation	$x_{14},x_{13},x_{12},x_{11},x_6$	$x_1,x_9,x_3,x_2,x_4,x_{10},x_8,x_5,x_7,\eta$	-3896375	6723
4	competition	cooperation	$x_{14},x_{13},x_{12},x_{11},x_6$	$x_1,x_3,x_2,x_{10},x_4,x_9,x_8,x_5,x_7,\eta$	-3924008	6599
5	competition	cooperation	$x_{14},x_{13},x_{12},x_{11},x_6,x_7,x_9$	$x_1,x_2,x_5,x_3,x_4,x_8,x_{10},\eta$	-3944530	6525
6	competition	cooperation	$x_{14},x_{13},x_{12},x_{11},x_6,x_9$	$x_1,x_3,x_2,x_4,x_5,x_8,x_{10},x_7,\eta$	-3951059	6495
7	competition	cooperation	$x_{14},x_{13},x_{12},x_{11},x_6,x_7,x_{10}$	$x_1,x_5,x_2,x_3,x_4,x_8,x_9,\eta$	-3956461	6455
8	competition	cooperation	$x_{14},x_{13},x_{12},x_{11},x_6,x_7,x_9$	$x_1,x_3,x_2,x_5,x_4,x_8,x_{10},\eta$	-3962558	6432
9	competition	cooperation	$x_{14},x_{13},x_{12},x_{11},x_6,x_7,x_{10}$	$x_1,x_2,x_3,x_4,x_5,x_8,x_9,\eta$	-3967305	6413
10	competition	cooperation	$x_{14},x_7,x_{13},x_{12},x_{11},x_6,x_9$	$x_1,x_3,x_4,x_2,x_5,x_8,x_{10},\eta$	-3970956	6574
11	competition	cooperation	$x_{14},x_{13},x_{12},x_{11},x_7,x_6,x_{10}$	$x_1,x_3,x_4,x_2,x_5,x_8,x_9,\eta$	-3969519	6406
12	competition	cooperation	$x_{14},x_{13},x_{12},x_{11},x_7,x_6,x_{10}$	$x_1,x_3,x_4,x_2,x_5,x_8,x_9,\eta$	-3969519	6406

TABLE 4. Iterative process for X_{Mass}.

Game rounds	Behavior of player		Strategy space		Objective function values	
	u_1	u_2	S_1	S_2	f_1 (kWh)	f_2 (kg)
Initial design	——	——	——	——	-3777346	7210
1	cooperation	competition	$x_{14},x_{13},x_{12},x_{11},x_{10},x_6$	$x_1,x_9,x_2,x_3,x_4,x_5,x_8,x_7,\eta$	-3807434	6029
2	cooperation	competition	$x_{14},x_{13},x_{12},x_{11},x_7,x_6$	$x_1,x_{10},x_2,x_3,x_4,x_5,x_8,x_9,\eta$	-3808943	5949
3	cooperation	competition	$x_{14},x_{13},x_{12},x_{11},x_7,x_6,x_9$	$x_1,x_3,x_{10},x_2,x_4,x_5,x_8,\eta$	-3809616	5910
4	cooperation	competition	$x_{14},x_{13},x_{12},x_{11},x_6,x_7$	$x_1,x_2,x_3,x_4,x_9,x_8,x_5,x_{10},\eta$	-3809486	5856
5	cooperation	competition	$x_{14},x_{13},x_{12},x_{11},x_6,x_7$	$x_1,x_9,x_3,x_2,x_{10},x_4,x_5,x_8,\eta$	-3810077	5802
6	cooperation	competition	$x_{14},x_{13},x_{12},x_{11},x_6,x_7$	$x_1,x_2,x_3,x_9,x_5,x_4,x_{10},x_8,\eta$	-3810617	5786
7	cooperation	competition	$x_{13},x_{14},x_{12},x_{11},x_6$	$x_1,x_2,x_{10},x_9,x_8,x_4,x_5,x_3,x_7,\eta$	-3810525	5769
8	cooperation	competition	$x_{14},x_{13},x_{12},x_{11},x_6,x_7$	$x_1,x_{10},x_2,x_3,x_4,x_8,x_9,x_5,\eta$	-3793071	5716
9	cooperation	competition	$x_{14},x_{13},x_{12},x_{11},x_6,x_7,x_5$	$x_1,x_9,x_2,x_8,x_3,x_4,x_{10},\eta$	-3810880	5757
10	cooperation	competition	$x_{14},x_{13},x_{12},x_{11},x_6,x_7,x_5$	$x_1,x_9,x_2,x_8,x_3,x_4,x_{10},\eta$	-3810880	5757

TABLE 5. Comparison of main performance parameters.

	AEP (kWh)	Mass (kg)	F_{max}(kN)	$\varepsilon_{max}(10^{-3})$	d_{max} (m)	f_{st} (Hz)	Game rounds
$X_{Initial}$	3777346	7210	64.7	3558	2.659	2.46	/
X_{AEP}	3969519	6406	69.5	4499	3.066	0.81	12
X_{Mass}	3810880	5757	63.6	4865	3.653	0.76	10

X_{AEP} = [3.2415, 2.6773, 2.3365, 2.1088, 1.8663, 1.6576, 1.3419, 0.1549, 0.1184, 0.0789, 0.0297, 0.0061, -0.0161, -0.0276, 36, 45, 56, 60, 51, 43, 35, 7.4857, 10.3458, 18.9036, 20.7837, 0.2490, 0.5811];

X_{Mass} = [3.1028, 2.5763, 2.1787, 1.9139, 1.7414, 1.4965, 1.1984, 0.1440, 0.0998, 0.0682, 0.0241, 0.0046, -0.0191, -0.0311, 28, 40, 50, 59, 49, 41, 30, 8.2231, 12.2900, 17.6724, 20.5673, 0.2473, 0.5104].

Compared to the initial design, the AEP of X_{AEP} solution increased by 192173 kWh and blade mass of the X_{AEP} solution decreased by 804 kg (Table 5). On the other hand, the AEP of the X_{Mass} solution increased by 33534 kWh and the blade mass decreased by 1453 kg. In addition, the X_{AEP} solution was superior to X_{Mass} in terms of AEP, but at the cost of a larger blade mass. The results suggest the design scheme is capable of representing the objective preferences of

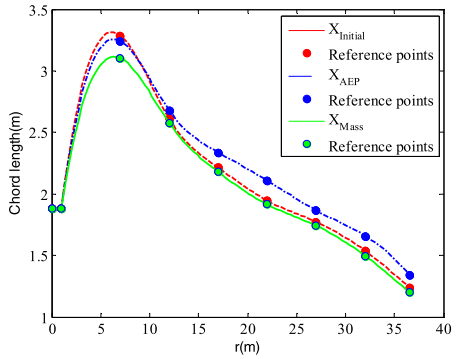

FIGURE 11. Chord length distribution of initial design, AEP preference (X_{AEP}) and blade mass preference (X_{Mass}).

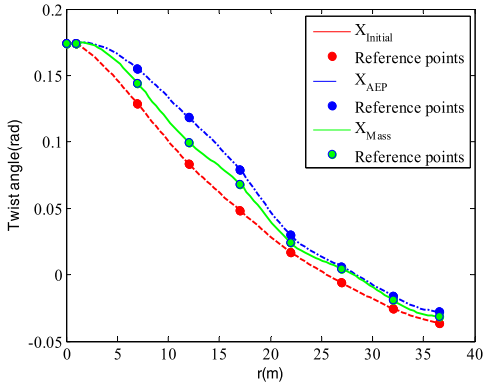

FIGURE 12. Twist angle distribution of initial design, AEP preference (X_{AEP}) and blade mass preference (X_{Mass}).

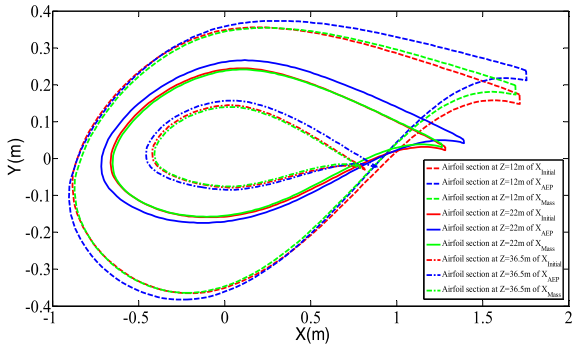

FIGURE 13. Airfoil section coordinates of initial design, AEP preference (X_{AEP}) and blade mass preference (X_{Mass}).

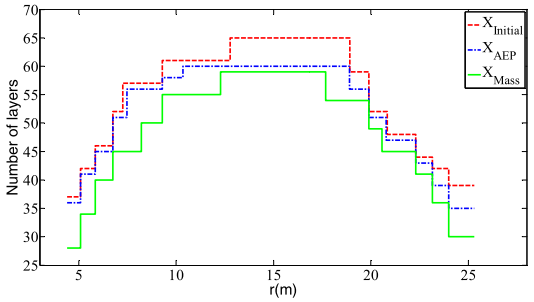

FIGURE 14. Spar cap layering of initial design, AEP preference (X_{AEP}) and blade mass preference (X_{Mass}).

the designer and clearly demonstrate the effectiveness of the proposed method. Moreover, the two optimized blade shapes presented in this paper were more reasonable. Comparisons of chord length distribution, twist angle distribution, airfoil section coordinates, and number of layers of the spar cap are shown in Figs 11–14.

Compared to the initial design, chord length of X_{AEP} from the root to transition area was shorter than that of the initial design, as shown in Fig. 11, and the blade chord length was longer in the most aerodynamic area, contributing to AEP increase. Furthermore, Fig. 11 reveals that the blade chord length of X_{Mass} is shorter than in the initial design, thereby helping to reduce the blade mass. Twist angles of both the X_{AEP} and X_{Mass} solutions from blade root to tip are larger than in the initial design, thus providing a better lift-to-drag ratio and improving the aerodynamic performance of the blade, as shown in Fig.12. In addition, the twist angle of the X_{AEP} solution is greater than that of the X_{Mass} solution, resulting in a higher AEP at the expense of blade mass for enabling the blade to withstand greater loads to meet the design constraints. Differences in chord length and twist angle are also reflected in the changes of airfoil section coordinates, as illustrated in Fig. 13, which shows coordinates of the nine different airfoil sections at Z = 12 m, 22 m, and 36.5 m. From Fig. 14, the number of layers of both the X_{AEP} and X_{Mass} solutions were lower compared to the initial design. These changes contribute to reducing blade mass. Moreover, the number of layers of the spar cap of X_{Mass} was lower than that of X_{AEP}, while the area containing the largest layer number had less layers than X_{AEP}. This also leads to a lower blade mass compared to the X_{AEP} solution. Additionally, the location of the shear web (x_{26}) was moved farther away from the center line of the cap, changing from 0.1333 m ($X_{Initial}$) to 0.2490 m (X_{AEP}) and 0.2473 m (X_{Mass}). Finally, the spar cap width (x_{27}) was reduced from 0.7135 m ($X_{Initial}$) to 0.5811 m (X_{AEP}) and 0.5104 m (X_{Mass}) which also contributes to the reduction of blade mass. These comparisons reveal the corresponding relationships between blade shape and two target preferences.

Table 5 shows that the maximum axial thrust of blade root (69.5kN for the X_{AEP} solution and 63.6kN for the X_{Mass} solution), maximum blade strain (0.004499 for the X_{AEP} solution and 0.004865 for the X_{Mass} solution), displacement of Y direction (3.066 m for X_{AEP} and 3.653 m for X_{Mass}), and first-order natural frequency (0.81 Hz for X_{AEP} and 0.76 Hz for X_{Mass}). The results satisfy all the constraints. To further show strain distribution of the blade, displacement in the Y direction and first vibration mode shape in detail, the X_{AEP} result are taken as an example and are shown in Fig. 15. From Fig. 15, (1) Strain values are higher in the spar cap compared to any other part of the blade, demonstrating that the spar cap is the main load-bearing component; moreover, larger strains occur near the middle of the blade; (2) Maximum displacement occurs at the blade tip and the blade will not damage the wind turbine tower; (3) The first natural vibration is the flap-wise mode and resonance can be avoided.

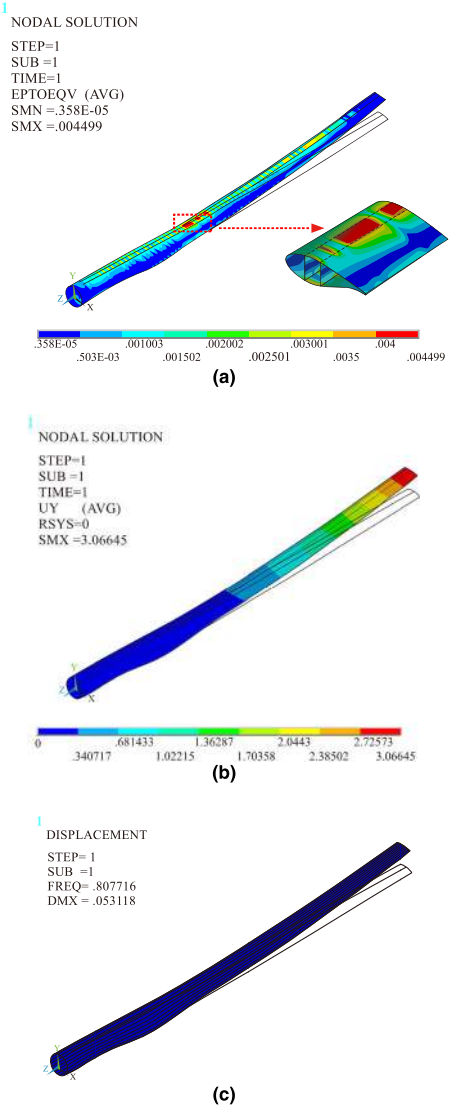

FIGURE 15. Blade's strain distribution(a), displacement of Y direction (b) and first vibration mode shape (c) of AEP preference (X_{AEP}).

C. DISCUSSION

The competitive-cooperative game method proposed in this paper has three main features below.

(1) Unlike equal status between players in [7], [8], [18], [22], the status of the two players in this study is unequal, and there is master-slave status. A player with competitive behavior cares only about personal profit, whereas a player exhibiting cooperative behavior also takes the benefit of other players into account while pursuing personal benefit. Therefore, the player of competitive behavior occupies the master's status, and the final game solution favors players who exhibit competitive behavior.

(2) The method brings out the corresponding relationships between blade shapes and solutions of two target preferences, and it is embodied by the fact that solution of X_{AEP} and X_{Mass} corresponds to the different chord length distribution, twist angle distribution, spar cap layering parameters, and airfoil section coordinates. These new findings cannot be drawn by these methods [7], [8], [18], [22].

(3) Different from the traditional static strategy space [7], [8], [18], game process of two players in this study is accompanied by the adjustment of strategy space, as clearly shown in Tables 3 and 4. A total of 21 different blade shapes were demonstrated, where x_{11}- x_{14} and x_6 always belongs to S_1 and x_1- x_4, x_8 and η always belong to S_2, while x_5, x_7, x_9, and x_{10} belong to S_1 or S_2. The results demonstrate that the twist angle between Z = 22.0 m and Z = 36.5 m and the chord length located at Z = 32 m have a significant influence on AEP for the 21 different blade shapes. On the other hand, the layering parameters (x_{15} - x_{25}), location of the shear web (x_{26}), spar cap width (x_{27}), chord length from Z = 7 m to Z = 22 m (x_1 - x_4), and twist angle near the transition area (x_8) have a significant influence on blade mass. In contrast, x_5, x_7, x_9, and x_{10} were adjusted for the various blade shapes. The dynamic adjustment of strategy space ensures that in each round of game, the strategy space of the players is composed of the design variables that have the relatively large influence on them. This ensures that a player's strategy adjustment will have a big impact on its profit, which is conducive to the in-depth game negotiation. Therefore, this dynamic strategy space is an improvement on the traditional static strategy space [7], [8], [18]. More deeply, unlike methods [7], [8], [18], [22], this method can assess the dynamic sensitivity of the design variables to the objective functions for different preference's blade shapes. For example, in descending order of sensitivity to AEP, S_1 is composed of the design variables x_{14}, x_{13}, x_{12}, x_{11}, x_7, x_6, and x_{10} for the final blade shape of the preferred AEP. In other words, changes in x_{14} cause the most significant changes to AEP, followed by x_{13}, x_{12}, x_{11}, x_7, x_6, and x_{10}. However, the order changes to x_{14}, x_{13}, x_{12}, x_{11}, x_6, x_7, and x_5 for the final blade shape of the preferred blade mass.

VI. CONCLUSION

A multi-objective optimization model of a HAWT blade was established based on its parameterized finite element model. 26 control points were used to simulate the laminate design of a spar cap. A novel competitive-cooperative game-theoretic method was proposed to obtain the optimal solution reflecting the designer's preferred objective. The proposed method comprises two new key techniques: (a) establishment of strategy space exploration method named 'correlation analysis under fuzzy k-means clustering', which can effectively divide design variables into strategy subspaces owned by each player with high partition efficiency. (b) construction of competitive-cooperative game pattern, which can not only guarantee collective benefit to all players, but also gives priority to players who exhibit competitive behavior. If the designer gives priority to structural performance of blade, then the structural objective is endowed with competitive behavior, and aerodynamic objective is given cooperative behavior, and vice versa. This method reduces the complexity of the problem by transforming a high-dimensional aerodynamic and structural optimization problem into two low-dimensional problems. Additionally, this method reveals

the corresponding relationships between blade shapes and solutions of two target preferences, and bring out the dynamic sensitivity of design variables to objective functions for the different blade shapes.

REFERENCES

[1] S. Y. D. Sorkhabi, D. A. Romero, G. K. Yan, M. D. Gu, J. Moran, M. Morgenroth, and C. H. Amon, "The impact of land use constraints in multi-objective energy-noise wind farm layout optimization," *Renew. Energy*, vol. 85, pp. 359–370, Jan. 2016.
[2] W. Long, R. Han, T. Wang, and S. Ke, "Uniform decomposition and positive-gradient differential evolution for multi-objective design of wind turbine blade," *Energies*, vol. 11, no. 5, p. 1262, May 2018.
[3] C. C. Liao, X. L. Zhao, and J. Z. Xu, "Blade layers optimization of wind turbines using FAST and improved PSO algorithm," *Renew. Energy*, vol. 42, no. 1, pp. 227–233, Jun. 2012.
[4] W. Hu, I. Han, S.-C. Park, and D.-H. Choi, "Multi-objective structural optimization of a HAWT composite blade based on ultimate limit state analysis," *J. Mech. Sci. Technol.*, vol. 26, no. 1, pp. 129–135, Jan. 2012.
[5] D. H. Wood, "Dual purpose design of small wind turbine blades," *Wind Eng.*, vol. 28, no. 5, pp. 511–527, Sep. 2004.
[6] A. Clarich, V. Pediroda, L. Padovan, C. Poloni, and J. Periaux, "Application of game strategy in multi-objective robust design optimisation implementing self-adaptive search space decomposition by statistical analysis," in *Proc. Eccomas*, Jyväskylä, Finland, 2004, pp. 1–20.
[7] C. Li and S. Li, "A computerized team approach for concurrent product and process design optimization," *Comput.-Aided Des.*, vol. 34, no. 1, pp. 57–69, Jan. 2002.
[8] R. Meng, K. H. Cheong, W. Bao, K. K. L. Wong, L. Wang, and N.-G. Xie, "Multi-objective optimization of an arch dam shape under static loads using an evolutionary game method," *Eng. Optim.*, vol. 50, no. 1, pp. 1061–1077, Oct. 2018.
[9] J. A. Désidéri, "Cooperation and competition in multidisciplinary optimization," *Comput. Optim. Appl.*, vol. 52, no. 1, pp. 29–68, May 2012.
[10] Y. Wang, H. Liu, W. Zheng, Y. Xia, Y. Li, P. Chen, K. Guo, and H. Xie, "Multi-objective workflow scheduling with deep-q-network-based multi-agent reinforcement learning," *IEEE Access*, vol. 7, pp. 39974–39982, 2019.
[11] Q. Feng, C. Hao, and Z. Chen, "Using game theory to optimize the allocation of defensive resources on a city scale to protect chemical facilities against multiple types of attackers," *Rel. Eng. Syst. Saf.*, vol. 191, Nov. 2017, Art. no. 105900.
[12] J. Gui, L. Hui, and N. Xiong, "A game-based localized multi-objective topology control scheme in heterogeneous wireless networks," *IEEE Access*, vol. 5, no. 1, pp. 2396–2416, 2017.
[13] J. Jiang and X. Liu, "Multi-objective Stackelberg game model for water supply networks against interdictions with incomplete information," *Eur. J. Oper. Res.*, vol. 266, no. 3, pp. 920–933, May 2018.
[14] R. Jing, M. Wang, H. Liang, X. Wang, N. Li, N. Shah, and Y. Zhao, "Multi-objective optimization of a neighborhood-level urban energy network: Considering game-theory inspired multi-benefit allocation constraints," *Appl. Energy*, vol. 231, pp. 534–548, Dec. 2018.
[15] N. I. Nwulu and X. Xia, "Multi-objective dynamic economic emission dispatch of electric power generation integrated with game theory based demand response programs," *Energy Convers. Manage.*, vol. 89, pp. 963–974, Jan. 2015.
[16] Y. Zhang, J. Wang, and Y. Liu, "Game theory based real-time multi-objective flexible job shop scheduling considering environmental impact," *J. Cleaner Prod.*, vol. 167, pp. 665–679, Nov. 2017.
[17] M. Xiao, X. Shao, L. Gao, and Z. Luo, "A new methodology for multi-objective multidisciplinary design optimization problems based on game theory," *Expert Syst. Appl.*, vol. 42, no. 3, pp. 1602–1612, Feb. 2015.
[18] N.-G. Xie, R. Meng, Y. Ye, L. Wang, and Y.-W. Cen, "Multi-objective design method based on evolution game and its application for suspension," *Struct. Multidisciplinary Optim.*, vol. 47, no. 2, pp. 207–220, Feb. 2012.
[19] M. Rui, N. Xie, and W. Lu, "Multiobjective game method based on self-adaptive space division of design variables and its application to vehicle suspension," *Math. Problems Eng.*, vol. 2014, no. 2, Jun. 2014, Art. no. 479272.
[20] X. Cai, *Wind Turbine Blades*. Beijing, China: China Water Power Press, 2013.
[21] J. Zhu, X. Cai, and R. Gu, "Aerodynamic and structural integrated optimization design of horizontal-axis wind turbine blades," *Energies*, vol. 9, no. 2, p. 66, Jan. 2016.
[22] R. Meng *et al.*, "Multi-objective aerodynamic and structural optimization of a wind turbine blade using a novel adaptive game method," *Eng. Optim.*, pp. 1–20, Sep. 2018. doi: 10.1080/0305215X.2019.1658749.
[23] F. Song, Y. Ni, and Z. Tan, "Optimization design, modeling and dynamic analysis for composite wind turbine blade," *Procedia Eng.*, vol. 16, no. 1, pp. 369–375, Dec. 2011.
[24] B. Bavanish and K. Thyagarajan, "Optimization of power coefficient on a horizontal axis wind turbine using BEM theory," *Renew. Sustain. Energy Rev.*, vol. 26, no. 26, pp. 169–182, Oct. 2013.
[25] P. Giguere and M. Selig, "Blade geometry optimization for the design of wind turbine rotors," presented at the ASME Wind Energy Symp., Carson City, NV, USA, no. 45, Aug. 2012.
[26] A. Kusiak, Z. Zhang, and M. Li, "Optimization of wind turbine performance with data-driven models," *IEEE Trans. Sustain. Energy*, vol. 1, no. 2, pp. 66–76, Aug. 2010.
[27] M. Jureczko, M. Pawlak, and A. M yk, "Optimisation of wind turbine blades," *J. Mater. Process. Technol.*, vol. 167, no. 2, pp. 463–471, Aug. 2005.
[28] J. Chen, Q. Wang, W. Z. Shen, X. Pang, S. Li, and X. Guo, "Structural optimization study of composite wind turbine blade," *Mater. Des.*, vol. 46, no. 4, pp. 247–255, Apr. 2013.
[29] Z. Sun, M. Sessarego, J. Chen, and W. Z. Shen, "Design of the OffWindChina 5 MW wind turbine rotor," *Energies*, vol. 10, no. 6, p. 777, Jun. 2017.
[30] G. B. Eke and J. I. Onyewudiala, "Optimization of wind turbine blades using genetic algorithm," *Global J. Res. Eng.*, vol. 10, no. 7, pp. 22–26, Dec. 2010.
[31] A. Arroyo, M. Manana, C. Gomez, I. Fernandez, F. Delgado, and A. F. Zobaa, "A methodology for the low-cost optimisation of small wind turbine performance," *Appl. Energy*, vol. 104, no. 2, pp. 1–9, Apr. 2013.
[32] W. Hu, K. K. Choi, and H. Cho, "Reliability-based design optimization of wind turbine blades for fatigue life under dynamic wind load uncertainty," *Struct. Multidisciplinary Optim.*, vol. 54, no. 4, pp. 953–970, Oct. 2016.
[33] J. F. Manwell, J. G. Mcgowan, and A. L. Rogers, *Wind Energy Explained: Theory, Design and Application*, 2nd ed. New York, NY, USA: Wiley, 2006.
[34] M. O. Hansen, *Aerodynamics of Wind Turbines*. New York, NY, USA: Routledge, 2015.
[35] T. Diveux, P. Sebastian, D. Bernard, J. R. Puiggali, and J. Y. Grandidier, "Horizontal axis wind turbine systems: Optimization using genetic algorithms," *Wind Energy*, vol. 4, no. 4, pp. 151–171, Oct. 2010.
[36] C. L. Bottasso, F. Campagnolo, and A. Croce, "Multi-disciplinary constrained optimization of wind turbines," *Multibody Syst. Dyn.*, vol. 27, no. 1, pp. 21–53, Jul. 2012.
[37] J. Jeong, K. Park, S. Jun, K. Song, and D.-H. Lee, "Design optimization of a wind turbine blade to reduce the fluctuating unsteady aerodynamic load in turbulent wind," *J. Mech. Sci. Technol.*, vol. 26, no. 3, pp. 827–838, Mar. 2012.
[38] K. Maki, R. Sbragio, and N. Vlahopoulos, "System design of a wind turbine using a multi-level optimization approach," *Renew. Energy*, vol. 43, pp. 101–110, Jul. 2012.
[39] W. Xudong, W. Z. Shen, W. J. Zhu, J. N. Sørensen, and C. Jin, "Shape optimization of wind turbine blades," *Wind Energy*, vol. 12, no. 8, pp. 781–803, Apr. 2009.

RUI MENG received the master's degree in engineering from the Anhui University of Technology, in 2009. He is currently pursuing the Ph.D. degree with Hohai University. Since 2009, he has been a Teacher with the School of Mechanical Engineering, Anhui University of Technology, where he is currently a Senior Engineer. His research interests include game theory, wind turbine blade design, multidisciplinary optimization design, and mechanical fault diagnosis.

NENG-GANG XIE received the Ph.D. degree in engineering from Hohai University, in 1999. He is currently a Professor and a Doctoral Supervisor with the Anhui University of Technology. He has published more than 140 articles in important academic journals, and presided over more than 30 scientific research projects. His research interests include multidisciplinary optimization design, game theory, and structure engineering.